International Journal of GEOMATE, Oct., 2022, Vol.23, Issue 98, pp.57-65
ISSN: 2186-2982 (P), 2186-2990 (O), Japan, DOI: https://doi.org/10.21660/2022.98.3438
Geotechnique, Construction Materials and Environment

RAPID MAGNITUDE ESTIMATION OF THE AUGUST 5, 2018, LOMBOK EARTHQUAKE USING HIGH-RATE GNSS DATA

*Irwan Meilano[1], Susilo Susilo[2] and Dina Sarsito[1]

[1]Faculty of Earth Science and Technology, Institute of Technology Bandung (ITB), Indonesia; [2]National Research and Innovation Agency (BRIN), Indonesia

*Corresponding Author, Received: 01 May 2022, Revised: 22 Aug. 2022, Accepted: 09 Oct. 2022

ABSTRACT: The rapid estimation of the magnitude of an earthquake is an essential part of an earthquake early warning system (EEWS), which is used to respond to earthquake shaking and the possible arrival of a tsunami. This research is the first in Indonesia to use Global Navigation Satellite System (GNSS) as part of an EEWS. Three high-rate GNSS datasets were processed using the precise point positioning post-processing method, which resulted in a peak ground displacement (PGD) and peak ground velocity (PGV) value due to the Lombok earthquake on August 5, 2018. The results showed that the magnitude of the PGD from the station closest to the earthquake source (KDOO) was Mw 6.6 within eight seconds of the original time, while that at the farthest location (CMAT) reached Mw 6.9 within 18 seconds of the original time. At the CMAT station, we also estimated the magnitude using PGV, which showed results consistent with the PGD data. These results confirm the potential use of the PGD and PGV data obtained from high-rate GNSS to estimate earthquake magnitudes rapidly as part of an EEWS.

Keywords: Earthquake magnitude, GNSS, PGD, PGV, Lombok

1. INTRODUCTION

In recent decades, Indonesia has experienced several earthquakes and tsunamis, including in Sumatra on December 26, 2004 (Mw 9.1), Mentawai on October 25, 2010 (Mw 7.8), and Palu on September 28, 2018 (Mw 7.5). Because these earthquakes and tsunamis have resulted in significant loss of life as well as economic losses, obtaining rapid magnitude information through EEWSs has become crucial. EEWSs speed up the decision-making process, thereby reducing the impact of earthquake shaking and tsunami evacuation process [1–2].

Typically, EEWSs use seismic data to estimate the main parameters of an earthquake, such as horizontal location, magnitude, and depth [3–6]. However, many studies have shown that using only seismic data for EEWSs can lead to magnitude saturation problems, especially for earthquakes with large magnitudes [4], [7–8]. The P wave in the initial seconds used to estimate the earthquake magnitude does not carry enough information to determine whether the earthquake will end as a magnitude 7, 8, or even 9. Furthermore, the time required to estimate the magnitude of an earthquake using seismic data relies heavily on the duration of the earthquake rupture process, which can be longer than 30 seconds for earthquakes above magnitude 8.

Research on and the implementation of GNSS in EEWSs have aimed to avoid magnitude saturated-related problems, such as the ShakeAlert system maintained by the United States Geological Survey (USGS) [9], Geodetic Alarm System [10], Bayesian Evidence-based Fault Orientation, Real-Time Earthquake-Slip [11], Geodetic First Approximation of Size and Timing [12], and Real-Time on the GNSS Earth Observation Network Analysis System for Rapid Deformation Monitoring [13]. GNSS can be conceptualized as a strong motion displacement sensor detecting long period waves, up to period 0 (static offset), so it can be an ideal complement to a seismometer.

The use of high-rate GNSS data to produce the waveform displacement required to capture the full complexity of ground motion has long been recognized [14–15]. This method enables real-time GNSS data and rapid magnitude to be obtained before the earthquake rupture is complete [8–16]. It is also used to obtain moment tensors [12], [17–18] and slip distribution [19–20]. Therefore, given the many potential benefits of high-rate GNSS data, they are now starting to become part of EEWSs [13], [21–22].

Although the use of GNSS as part of EEWSs has become increasingly popular, it has never been implemented in Indonesia, whose earthquake sources have various mechanisms. This research is the first in Indonesia to carry out a test using high-rate GNSS observations from the 2018 back-arc thrust zone Lombok earthquake. The analysis was carried out in three HR-GNSS stations during the earthquake (Mw 6.9 on August 5, 2018; 11:46:37 UTC) [23]. The Meteorological, Climatological,

and Geophysical Agency (BMKG) stated that the August 5, 2018, Lombok earthquake was the mainshock, while the earthquake on July 28, 2018, was the preshock. It released a tsunami warning for the second earthquake, later canceled at 13:25 UTC [23].

Unlike countries implementing an EEWS, Indonesia has a limited network of seismometers and GNSS observations. For example, Japan has one CGPS for every 280 square kilometers, while Indonesia has about one for every 9,000 square kilometers. The limited number of CGPS observation points will affect the speed and accuracy of the earthquake magnitude estimation. In addition, the earthquake source and the CGPS point will be far apart, and there will be a minimum detectable magnitude limit on a network with a small number of observations. This study uses the case of the 2018 Lombok earthquake, with a magnitude of 6.9. This case provides important information on preparing the EEWS based on GNSS data, especially for the case of an earthquake of a small magnitude and a limited number of observation stations.

2. DATA AND METHODS

This study analyzed three GNSS data recorded on the island of Lombok (Fig. 1). The CMAT point, which is located in the southwestern part of the island, is used as part of the Indonesian Continuously Operating Reference Station network managed by the Indonesian Geospatial Information Agency. The KDOO and PGRJ points located in the northern part of Lombok are continuous GNSS stations installed by the Faculty of Earth Science and Technology. All observation points have the capability to observe GNSS data in high frequency (1 Hz).

The CMAT station is located ~52 km from the epicenter of the second Lombok earthquake (Mw 6.9), while the KDOO and PGRJ are located about ~12 km and ~24 km away, respectively. The observation network, which is located far from the earthquake source and has a small number of points, is not ideal for detecting earthquakes with a magnitude below 7. However, this study provides a unique opportunity to test the capability of GNSS as part of an EEWS with limited network conditions.

The data-processing code derived from the precise point positioning approach described by [26–27] was used to obtain a 1 Hz coordinate time series solution. In addition to this approach, the final satellite orbit, phase and bias clocks, and a second ionospheric correction product generated by GeoForschungs Zentrum were used to obtain a coordinate solution to resolve integer ambiguities. The latest International GNSS Services antenna phase center model, code bias model, solid earth tide, ocean tidal displacement, and pole tide model were also used. The Vienna Mapping Function 3 [28] was used to project tropospheric zenith delays in slanting directions.

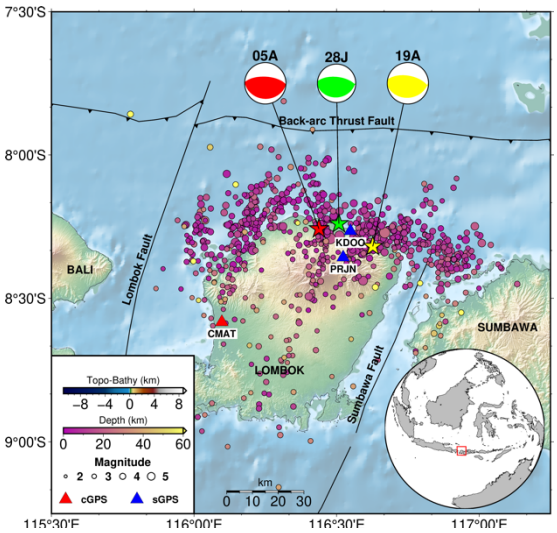

Fig. 1 The distribution of the three HR-GNSS stations and earthquake epicenters. The focal mechanisms and earthquake locations are obtained from the USGS, with 28J (July 28, 2018), 05A (August 5, 2018), and 19A (August 19, 2018). The colored circles represent the aftershock events [24] and the topography data from the Shuttle Radar Topography Mission (SRTM15+V2.1) [25]. Inset is the regional position of the study area in Indonesia.

The global coordinates solution with respect to International Terrestrial Reference Frame 2014 [29] were projected into topographical coordinates to derive the local waveform displacements in the north, east, and up components, as shown in Figs. 2–4. Using Equation (1), the PGD value is calculated based on the three-component displacement waveform [8]:

$$\boldsymbol{PGD} = \sqrt{\boldsymbol{n_d(t)^2} + \boldsymbol{e_d(t)^2} + \boldsymbol{u_d(t)^2}} \quad (1)$$

with the PGD in meters. Here, $\boldsymbol{n_d(t)}$, $\boldsymbol{e_d(t)}$, and $\boldsymbol{u_d(t)}$ are the north, east, and up waveform displacements at time t, respectively. Rapid earthquake moment as a function of rupture time is calculated using the relation formula between the moment magnitude and PGD proposed by [8], as shown in equation (2)

$$\boldsymbol{log(PGD)} = \boldsymbol{A} + \boldsymbol{B} \times \boldsymbol{M_w} + \boldsymbol{C} \times \boldsymbol{M_w} \times \boldsymbol{log}\,(\boldsymbol{R}) \quad (2)$$

where A, B, and C denote the regression coefficients, M_w is the moment magnitude, and R is the hypocentral distance from the GNSS observation station to the earthquake source in km.

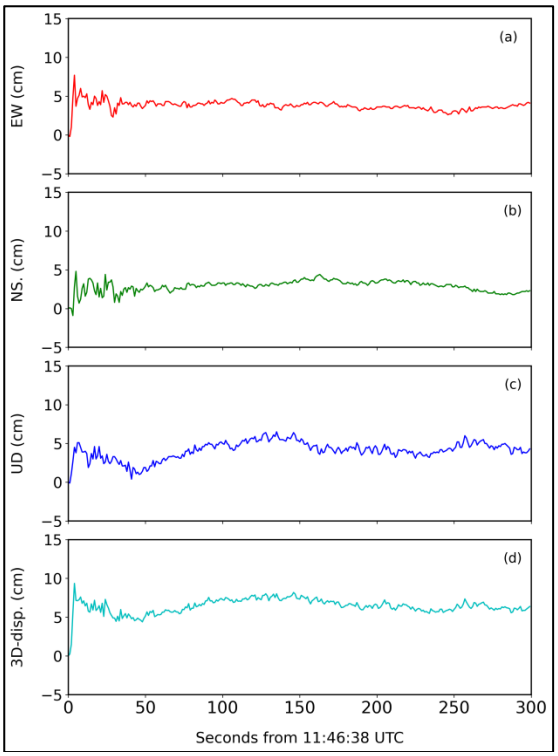

Fig. 2 KDOO waveform displacements: (a) north–south (NS), (b) east–west (EW), (c) up–down (UD), and (d) 3D displacement from the original time (11:46:37 UTC).

Furthermore, the regression coefficients obtained from [21], with values of -6,687, 1500, and -0.214 for A, B, and C, respectively, were used to determine the moment magnitude using the displacement waveform PGD. The standard error of magnitude estimation is 0.27 magnitude units. The regression parameters are built on worldwide observations, but most subduction zone earthquake events are not recorded by the GNSS at hypocenter distances less than 80 km. Therefore, the current regression parameters may not be fully appropriate for the 2018 Lombok earthquake.

3. RESULTS

Using waveform displacement time series (Figs. 2–4), the static horizontal coseismic offset was calculated by subtracting the average displacement between 50 and 300 s from the value at the original time (Fig. 5). Static offset data can be used to estimate coseismic slip distribution in the earthquake fault plane. The slip distribution information becomes the input for the calculation of a realistic earthquake magnitude and is used as a comparison for the rapid calculation of the earthquake magnitude. The maximum static offset for 05A was 3.8 cm, 4.0 cm, and 8.1 cm for the KDOO, PGRJ, and CMAT stations, respectively.

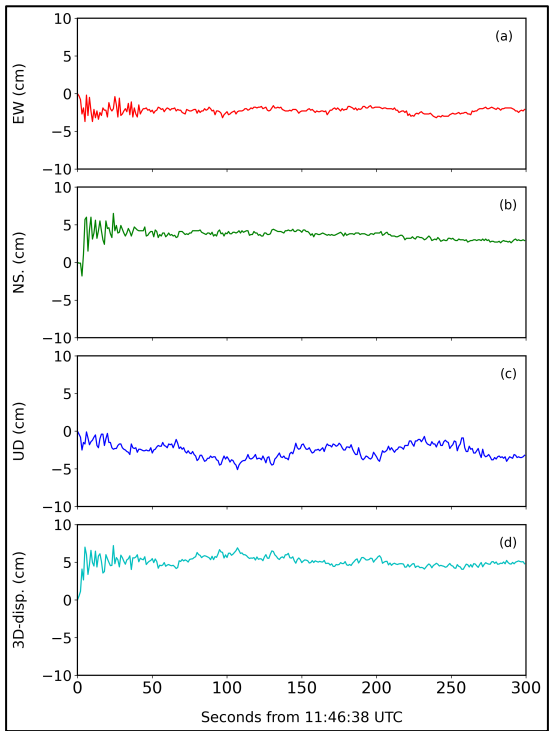

Fig. 3 PGRJ waveform displacements: (a) north–south (NS), (b) east–west (EW), (c) up–down (UD), and (d) 3D displacement from the original time (11:46:37 UTC).

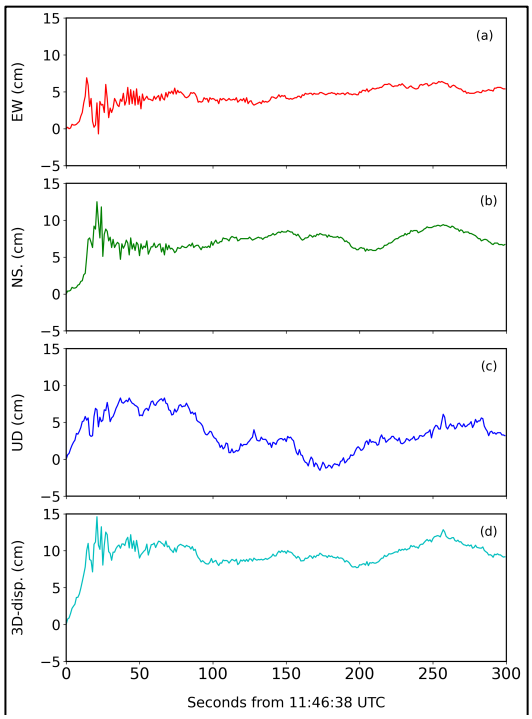

Fig. 4 CMAT waveform displacements: (a) north–south (NS), (b) east–west (EW), (c) up–down (UD), and (d) 3D displacement from the original time (11:46:37 UTC)

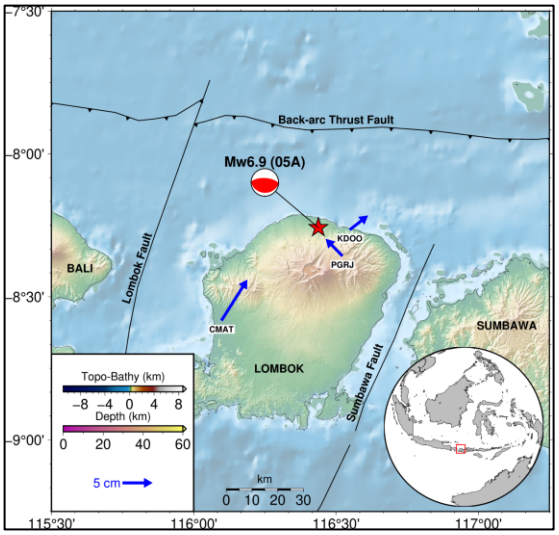

Fig. 5 The horizontal coseismic static offset calculated from the average waveform displacement.

The static offset estimated from the vertical component has a higher signal-to-noise ratio than that of the horizontal component. Therefore, horizontal data is used to analyze the distribution of slips. The CMAT offset confirms the previous report [30] using the GNSS method of static daily solutions. The results from the daily solution may be influenced by short-term postseismic deformation, and averaging the initial data from high-rate observations will produce more realistic coseismic values.

Northward displacement was detected at all the observation stations. The deformation pattern showed that the earthquake had a vertical fault mechanism and was related to the activity of the Flores back-arc thrust [30]. It is interesting to note that the most considerable coseismic offset value was detected at the observation point furthest away from the earthquake epicenter (CMAT). This indicates that the back-arc thrust earthquake slip is not only concentrated in the north but also reaches the south. And the magnitude of the slip in the south is indicated to be greater than in the north.

The displacement time series (Figs. 2–4) for the CMAT and PGRJ observation points showed that the vertical component was less sensitive to the Lombok earthquake. Vertical deformation was only detected at the KDOO observation point, less than five seconds after earthquake initiation. This indicates the beginning of the earthquake rupture starting in the north. Then, the slip spreads to the south, where the lower end of the earthquake fault plane does not reach the observation stations in the south (PGRJ and CMAT). All observation stations detect earthquake shaking with a duration of not less than 50 seconds. The most prolonged shock detected was in CMAT, over 75 seconds, which could indicate that the slip was longer or that the local site effect implicated the duration of the shaking. The trend of the PGD magnitude was calculated using the 3D waveform displacements and hypocentral distances. The average PGD magnitudes were 6.4, 6.4, and 6.9 from the KDOO, PGRJ, and CMAT 3D waveform displacements, respectively (Fig. 6). The estimation results from the three observation stations showed a difference in magnitude of 0.5. This difference was also found in the analysis of the Aegean Sea (Mw 6.58) and Mentawai (Mw 7.49) earthquakes [16].

The difference in magnitude could be due to the regression parameters used [21] for the mechanism of the thrust fault earthquake from the observation point further than 40 km [16], as the distance between the KDOO and PGRJ stations was less than 15 km for the Lombok earthquake. The distance from the CMAT observation point to the epicenter was about 52 km, a distance at which the magnitude was close to the estimate from the seismic data. Another possible cause of the difference in magnitude values is the regression parameter used [21], which is estimated based on earthquake data with a magnitude above Mw 7.5 and has low sensitivity for smaller earthquakes.

An earthquake with a magnitude close to 7 has a source time function of fewer than 40 seconds. In the case of the Aegean Mw 6.87 earthquake, the time required to estimate the magnitude based on PGD data is 40 seconds [21]. This study resulted in a faster magnitude estimate (Fig. 6) at 8–18 seconds. This is because the GNSS observation network used in this study is very close to the earthquake's epicenter.

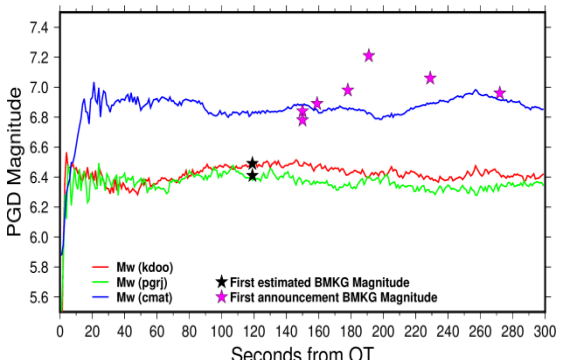

Fig. 6 Time series PGD magnitude from the 3D waveform displacement for each site and BMKG magnitude estimation.

The magnitude comparison is shown in Table 1, which shows that the initial estimated magnitude from the BMKG was Mw 6.4 at 120 seconds after the earthquake. This is an underestimation of the true magnitude and is similar to the initial estimate of 8 seconds from the GNSS observations. The BMKG updated the earthquake magnitude at 150

seconds, which resulted in a magnitude of Mw 6.8; this result is similar to the PGD results at the CMAT station at 18 seconds. A more stable magnitude estimation result from various international institutions (GCMT and USGS) is Mw 6.9, but it needs a longer computational time because it requires observation data from more seismic networks from various regions of the world. Earthquake magnitude can also be estimated based on PGV data using a regression model [21]. To obtain the site velocity time series, we used a variometric approach implemented in the SNIVEL software [32].

Table 1 Magnitude comparison

Magnitude (Mw)	Reference	Remark
6.4	BMKG	1st Estimat
7.0	BMKG	Update
6.9	GCMT	-
6.9	USGS	-
6.4	This study	KDOO average
6.4	This study	PGRJ average
6.9	This study	CMAT average

Figs. 7 and 8 show the velocity waveform at the CMAT stations. After the earthquake, all the components experienced fluctuating velocity, with vertical velocities less sensitive than horizontal velocities. The results from horizontal velocity are relatively more sensitive to earthquake signals than displacement observations (Fig. 7). Seismic signal patterns are seen in all components from the horizontal direction, with the maximum value detected at 18 seconds. The vertical component of velocity can detect seismic signals better than using displacement observation data. Fig. 7 shows that the velocity time series does not show significant fluctuations and the noise level is rather constant. This time series characteristic of the velocity allows the detection of seismic waves using a simple filtering process. We extract the PGV from the three-component velocity waveform as

$$\boldsymbol{PGV} = \sqrt{\boldsymbol{n_v(t)^2 + e_v(t)^2 + u_v(t)^2}} \qquad (3)$$

where $n_v(t)$, $e_v(t)$, and $u_v(t)$ are the north, east, and top velocity waveforms, respectively. After the regression coefficients were determined, we applied the PGV scaling law to calculate the earthquake magnitude. The maximum magnitude of PGV (Fig. 8) was 6.5 cm/s, using a regression coefficient (A = 5.025, B = 0.741, and C = 0.111) [31], resulting in an Mw value of 6.97. These results indicate that for the CMAT stations, both the PGD and the PGV can provide reasonable estimates of earthquake magnitudes that are consistent with those obtained from seismological methods. Results [33] for magnitude estimation using only one CMAT station produce a magnitude value of Mw 6.6 in the first 10 seconds. Using a single station [33] has a disadvantage because the geometric constraint in estimating the magnitude parameter is very weak.

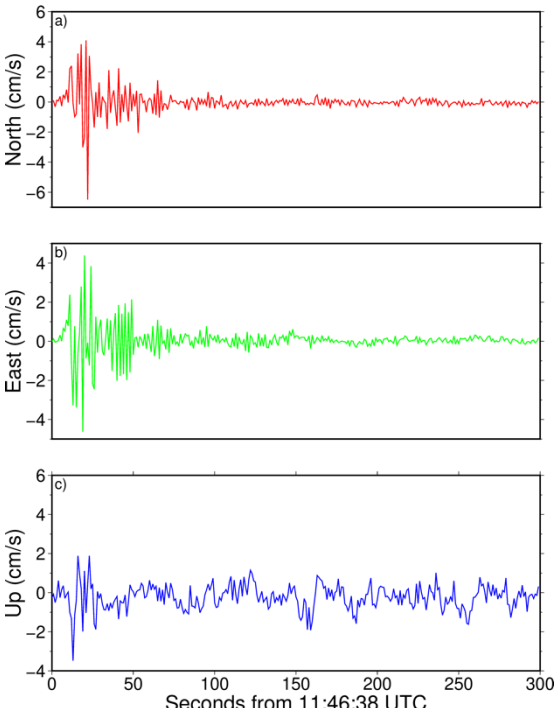

Fig. 7 Velocity time series results at the CMAT stations.

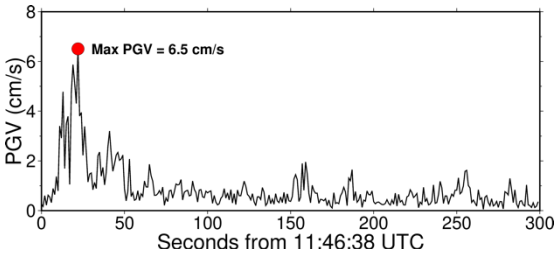

Fig. 8 PGV results at the CMAT stations. The red dot shows the maximum observed PGV.

4. DISCUSSION

4.1 Magnitude Estimation from Static Analysis

The moment magnitude of the earthquake is estimated using the distribution of the slip on the earthquake plane. The slip distribution of earthquakes is heterogeneous and depends on the stress conditions and rock mechanic properties. The slip distribution from an earthquake reflects the stress release during an earthquake and helps detect changes in stress in the surrounding area [34]. We modeled the static offset displacement (Fig. 5) using fault dislocations in a homogeneous elastic

half-space [35]. We fixed the depth, strike, and dip angle of the fault according to [36]. We employ a 3 x 3 km discretization of the fault plane. Our analysis suggests that the earthquake has a maximum coseismic slip of 200 cm (Fig. 9) and earthquake magnitude of Mw 6.92. This estimated coseismic slip is larger than the estimation from InSAR data [36], but consistent with the result obtained by USGS. This difference is probably due to the very limited number of GNSS observation data used in the inversion process.

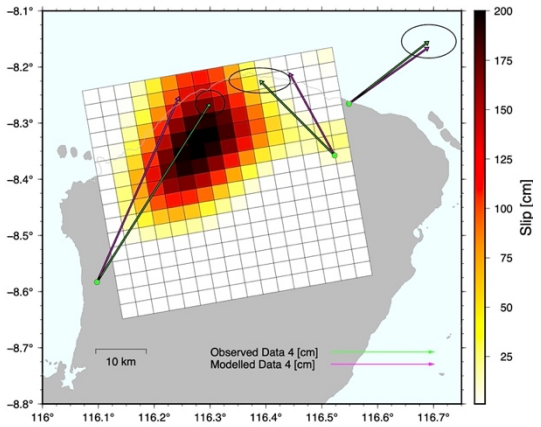

Fig. 9 Coseismic slip distribution obtained from static offset displacement.

The magnitude estimation results using static data are consistent with the results from high-rate analysis. These results show that, although the rapid estimation cannot be used to calculate the slip distribution, the magnitude estimation obtained, even with a limited number of observations, is adequate to be used as a basis for earthquake early warning.

4.2 Real-Time Implementation

This warning system will be helpful if it can detect and characterize earthquake events quickly. However, it must be able to disseminate quickly. It can then be used as a basis for decision-making by the community. This study uses a post-processing algorithm in its analysis, and it is a challenge to be able to do it in real time.

We also analyzed the time required to estimate the earthquake magnitude from HR-GNSS using only the CMAT station data. The BMKG seismic station detected event 05A within 69 seconds (1.15 minutes) of the original time. BMKG automatically estimated the initial magnitude of Mw 6.41 at 118–119 seconds (~1.98 minutes), officially released at 150 seconds (~2.5 minutes) after the original time (Fig. 6). Meanwhile, the CMAT PGD reached Mw 6.9 within 18–20 seconds of the original time, with an average magnitude of 6.9.

These results show that the time needed to estimate the magnitude of the PGD is less than that needed to estimate the magnitude of the seismology. This result is achieved by kinematic post-processing, when all the data, orbit, and clock corrections are already available, which takes time to set up. Methods based on GNSS data have the potential to complement seismic observations. To implement this method in real time, we must consider the quality of the communication data from the GNSS station to the processing server, real-time processing methods, and various factors related to the type of orbit. In addition, we must build a regression coefficient that includes observations close to the earthquake source.

The 1 Hz CGPS observation data can contribute to the EEWS by estimating the PGD magnitude scaling and PGV. In addition, because PGVs correlate well with damage and shaking intensity, it is very important to be able to estimate it in real time.

5. CONCLUSION

This research used GNSS waveform displacements to estimate the magnitude of the Lombok earthquake that occurred on August 5, 2018, using the PGD and PGV scaling law. The results showed that, using the post-processing method, the PGD and PGV magnitude of this earthquake reached Mw 6.9 within 18 seconds of the original time, with an average value of Mw 6.9 from ~5 minutes of data. The value of this magnitude is confirmed by the slip distribution obtained from the inversion of static GNSS data processing. Further studies must be carried out to find ways to estimate the PGD magnitude in real time based on the quality of the communication data, real-time GNSS processing methods, and distributions of the GNSS stations.

6. ACKNOWLEDGEMENTS

We thank Geospatial Information Agency for providing continuous GNSS data. This research was partially funded by the ITB Research Grant 2022 (PN-6-05-2022) and Indonesia Endowment Fund for Education (LPDP) (Grant number S-303/LPDP.4/2022).

7. REFERENCES

[1] Kanamori H., Real-Time Seismology and Earthquake Damage Mitigation. Annual Review of Earth and Planetary Sciences, vol. 33, No. 1, 2004, pp. 195–214.

[2] Allen R. M. and Melgar D., Earthquake Early Warning: Advances, Scientific Challenges, and Societal Needs. Annual Review of Earth and Planetary Sciences, vol. 47, No. 1, 2019, pp. 361–388.

[3] Allen R. M. and Kanamori H., The Potential for Earthquake Early Warning in Southern California. Science, vol. 300, No. 5620, 2003, pp. 786–789.
[4] Wu Y. M. and Zhao L., Magnitude Estimation Using The First Three Seconds P-Wave Amplitude In Earthquake Early Warning. Geophysical Research Letters, vol. 33, No. 16, 2006, pp. 1-4.
[5] Zollo A., Lancieri M., and Nielsen S., Earthquake Magnitude Estimation From Peak Amplitudes Of Very Early Seismic Signals On Strong Motion Records. Geophysical Research Letters, vol. 33, no. 23, 2006, pp. 1-6.
[6] Peng, J. S. Yang, Zheng Y., Zhu X. Y., Xu Z. Q., and Chen Y., New Tc Regression Relationship Derived From All P Wave Time Windows For Rapid Magnitude Estimation. Geophysical Research Letters, vol. 44, No. 4, 2017, pp. 1724–1731.
[7] Brown H. M., Allen R. M., Hellweg M., Khainovski O., Neuhauser D., and Souf A., Development of the ElarmS methodology for earthquake early warning: Realtime application in California and offline testing in Japan. Soil Dynamics and Earthquake Engineering, vol. 31, no. 2, 2011, pp. 188–200.
[8] Crowell B. W., Melgar D., Bock Y., Haase J. S., and Geng J. Earthquake magnitude scaling using seismogeodetic data. Geophysical Research Letters, vol. 40, no. 23, 2013, pp. 6089–6094.
[9] Given D. D., Technical Implementation Plan For The Shakealert Production System: An Earthquake Early Warning System For The West Coast Of The United States. Reston, VA, 2014, pp. 1155.
[10] Grapenthin R., Johanson I. A., and Allen R. M. Operational real-time GPS-enhanced earthquake early warning. Journal of Geophysical Research: Solid Earth, vol. 119, No. 10, 2014, pp. 7944–7965.
[11] Minson S. E., Murray J. R., Langbein J. O., and Gomberg J. S., Real-time inversions for finite fault slip models and rupture geometry based on high-rate GPS data. Journal of Geophysical Research: Solid Earth, Vol. 119, No. 4, 2014, pp. 3201–3231.
[12] Melgar D., Bock Y., and Crowell B. W., Real-time centroid moment tensor determination for large earthquakes from local and regional displacement records. Geophysical Journal International, Vol. 188, No. 2, 2012, pp. 703–718.
[13] Kawamoto S., Ohta Y., Hiyama Y., Todoriki M, Nishimura T., Furuya T., Sato Y., Yahagi T., Miyagawa K., REGARD: A new GNSS-based real-time finite fault modeling system for GEONET. Journal of Geophysical Research: Solid Earth, Vol. 122, No. 2, 2017, pp. 1324–1349.
[14] Bock Y. and Melgar D., Physical applications of GPS geodesy: a review. Reports on Progress in Physics, Vol. 79, No. 10, 2016, pp. 106801.
[15] Larson K. M., Unanticipated Uses of the Global Positioning System. Annual Review of Earth and Planetary Sciences, Vol. 47, No. 1, 2019, pp. 19–40.
[16] Melgar D., Seismogeodesy of the 2014 Mw6.1 Napa earthquake, California: Rapid response and modeling of fast rupture on a dipping strike-slip fault. Journal of Geophysical Research: Solid Earth, vol. 120, no. 7, Jul. 2015, pp. 5013–5033
[17] Riquelme S., Bravo F. J., Melgar D., Benavente R. F., Campos J. A., W phase source inversion using high-rate regional GPS data for large earthquakes. Geophysical Research Letters, Vol. 43, No. 7, 2016, pp. 3178–3185.
[18] O'Toole T. B., Valentine A. P., and Woodhouse J. H., Centroid–moment tensor inversions using high-rate GPS waveforms. Geophysical Journal International, Vol. 191, No. 1, 2012, pp. 257–270.
[19] Crowell B. W., Bock Y., and Melgar D., Real-Time Inversion of GPS Data For Finite Fault Modeling And Rapid Hazard Assessment. Geophysical Research Letters, Vol. 39, No. 9, 2012, pp. 1-6.
[20] Wright T. J.,Houlié N.,Hildyard M., and Iwabuchi T., Real-time, reliable magnitudes for large earthquakes from 1 Hz GPS precise point positioning: The 2011 Tohoku-Oki (Japan) earthquake. Geophysical Research Letters, Vol. 39, No. 12, 2012, pp. 1-5.
[21] Crowell B. W.., Demonstration of the Cascadia G‐FAST Geodetic Earthquake Early Warning System for the Nisqually, Washington, Earthquake. Seismological Research Letters, vol. 87, no. 4, Jun. 2016, pp. 930‐943.
[22] Murray J. R. et al., Development of a Geodetic Component for the U.S. West Coast Earthquake Early Warning System. Seismological Research Letters, vol. 89, no. 6, Oct. 2018, pp. 2322–2336.
[23] Yudi A., Santoso E., Kaluku A., and Artadi Pria Sakti D. P., Sigit P., Ulasan Guncangan Tanah Akibat Gempa Lombok Timur 05 Agustus 2018. Badan Metalurgi, Klimatologi dan Geofisika, 2018. https://prosesweb.bmkg.go.id/wp-content/uploads/Ulasan-Guncangan-Gempa-Lombok - Timur-29072018.pdf (accessed Sep. 13, 2021).
[24] Supendi P. et al., Relocated aftershocks and background seismicity in eastern Indonesia shed light on the 2018 Lombok and Palu earthquake sequences. Geophysical Journal International, Vol. 221, No. 3, 2020, pp. 1845–1855.

[25] Tozer B., Sandwell D. T.. Smith W. H. F, Olson C., Beale J. R., and Wessel P., Global Bathymetry and Topography at 15 Arc Sec: SRTM15+. Earth and Space Science, Vol. 6, No. 10, Oct. 2019, pp.1847–1864.

[26] Geng J. et al., PRIDE PPP-AR: An Open-Source Software for GPS PPP Ambiguity Resolution. GPS Solut., vol. 23, no. 4, Oct. 2019, pp. 1–10.

[27] Geng J., Chen X., Pan Y., and Zhao Q., A modified phase clock/bias model to improve PPP ambiguity resolution at Wuhan University. Journal of Geodesy, vol. 93, no. 10, 2019, pp. 2053–2067.

[28] Landskron D. and Böhm J., VMF3/GPT3: refined discrete and empirical troposphere mapping functions. Journal of Geodesy, vol. 92, no. 4, 2018, pp. 349–360,

[29] Altamimi Z., Rebischung P., Métivier L., and Collilieux X., ITRF2014: A new release of the International Terrestrial Reference Frame modeling nonlinear station motions. Journal of Geophysical Research: Solid Earth, vol. 121, no. 8, Aug. 2016,pp. 6109–6131.

[30] Susilo S. et al., GPS/GNSS Analysis On Lombok Earthquakes: Co-Seismic Deformation. 2018, doi: 10.13140/ RG.2.2.34871.78242.

[31] Pakhrur R, Josaphat T. S., Joko W., Yuta I. and Daniele P., Land Deformation Monitoring Using D-Insar Technique During Lombok Earthquake Observed By Sentinel-1a/B. International Journal of GEOMATE, Sept., 2020,Vol.19, Issue 73, pp.257-262

[32] Fang R., Zheng J., Geng J., Shu Y., C. Shi, J. Liu, Earthquake magnitude scaling using peak ground velocity derived from high-rate GNSS observations. Seismological Research Letters, 92, 2021, pp 227–237.

[33] Susilo., Meilano I., Hardy T., Kautsar M.A., Sarsito D., Efendi J., Rapid Estimation of Earthquake Magnitude using GNSS Data, IOP Conf. Ser.: Earth Environ. Sci. 873 012063, 2021, doi:10.1088/1755-1315/ 873/1/012063

[34] Meilano I., Salman R., Rahmadani S., Shi Q., Susilo S., Lindsey E., Supendi P., ; Daryono D., Source Characteristics of the 2019 Mw 6.5 Ambon, Eastern Indonesia, Earthquake Inferred from Seismic and Geodetic Data, Seismological Research Letters, 2021, 92 (6): 3339–3348, https://doi.org/10.1785/0220210021

[35] Okada Y., Surface deformation due to shear and tensile faults in a half-space, Bulletin of the Seismological Society of America, 1985 75 (4): 1135–1154, https://doi.org/10.1785/ BSSA0750041135

[35] Salman R., Eric O. Lindsel, Karen H. Lythgoe, Kyle Bradley, Muzli Muzli, Sang‐Ho Yun, Shi Tong Chin, Cheryl W. J. Tay, Fidel Costa, Shengji Wei, Emma M. Hill, Seismological Research Letters, 2020, 91 (4): 2141‐215, https://doi.org/10.1785/ 0220190378